Electronic Supplementary Material (ESI) for Materials Horizons.
This journal is © The Royal Society of Chemistry 2020

Supporting Information

Enhanced Charge Separation and Photocatalytic Hydrogen Evolution in Carbonized-Polymer-Dots-Coupled Lead Halide Perovskites

Yue Zhao,‡[a] Qingsen Zeng,‡[a] Yue Yu, [a] Tanglue Feng, [a] Yajie Zhao,[b] Zidong Wang,[a] Yi Li,[b] Chongming Liu,[a] Junjun Liu,[a] Haotong Wei,[a] Shoujun Zhu,[a] Zhenhui Kang,*[b] Hao Zhang[a] and Bai Yang*[a]

[a]*State Key Laboratory of Supramolecular Structure and Materials, College of Chemistry, Jilin University, Changchun 130012, China.*
E-mail: byangchem@jlu.edu.cn

[b]*Institute of Functional Nano and Soft Materials (FUNSOM), Jiangsu Key Laboratory for Carbon-based Functional Materials and Devices, Soochow University, Suzhou 215123, China.*
E-mail: zhkang@suda.edu.cn

Table of contents in Supporting Information

Experiments and methods

Chemicals and materials. PbI_2 (98%), HI (8.3-8.7 mol L^{-1}, 55-58 wt%, in water, 1.5% H_3PO_2-stabilized), methylamine (40% in methanol), $H_2PtCl_6 \cdot 6H_2O$, H_3PO_2 (50 wt%, in water), graphene, anhydrous citric acid (CA, 98%), ethanediamine (EDA), o-phenylenediamine (OPDA) and nickel acetate ($NiC_4H_6O_4 \cdot 4H_2O$) were purchased from Aladdin. P-Aminosalicylic acid (PASA, 99%) was obtained from J&K Scientific Ltd. Black phosphorus nanosheets (BP, 0.2 mg/mL in water) were achieved from XFNANO. Oleylamine was obtained from Sigma Aldrich. Commercial TiO_2 nanocrystals (P25) were obtained from Macklin. Toluene, DMF, DMSO, n-hexane, isopropanol, acetone, and methyl alcohol were purchased from Beijing Chemical Works. All chemicals were used as received.

Synthesis of methylammonium iodide (MAI). MAI was prepared by reacting a 1:1 molar ratio of methylamine and HI. The reacting solution was stirred at 0 ^{o}C for 2 h. The solvent was removed by rotary evaporation at 60 ^{o}C for 1 h. The precipitates were dissolved in ethanol, and diethyl ether was added to precipitate the MAI. This purification process was repeated twice. After purification, the product was dried in a vacuum oven at 60 ^{o}C for 24 h.

Preparation of $MAPbI_3$ powders and $MAPbI_3$-Saturated HI Solution. $MAPbI_3$ was synthesized by dissolving MAI and PbI_2 with molar ratio of 1:1 in aqueous solution.[1] In detail, 15 g of PbI_2 was dissolved in the mixed solution of 40 mL of HI acid and 10 mL of H_3PO_2 acid, then 5.17 g of MAI was slowly added into above solution with vigorous stirring under 60 ^{o}C. The solution with excess black powder was heated to 100 ^{o}C and kept for 1 h to crystallize and reach dynamic equilibrium, then cooled down to room temperature to obtain saturated solution with black $MAPbI_3$ precipitates. The $MAPbI_3$ precipitates were separated from saturated solution by centrifugation and dried in a vacuum oven at 60 ^{o}C to get $MAPbI_3$ powders, and obtained saturated solution was preserved for next operation and measurement. The reaction process was protected with N_2 gas.

Preparation of CA-PASA CPDs with yellow-green emission. The CA-PASA CPDs was synthesized according to the modified recipe of our previous work.[2] Citric acid (CA) (1 mmol) and p-aminosalicylic acid (1 mmol) were dissolved in 10 mL of water, and the pH was adjusted by concentrated hydrochloric acid to about 1. Then the mixture was heated at 200 ℃ for 8 h in a poly(tetrafluoroethylene) (Teflon)-lined autoclave. After cooling down, the as-prepared solution was filtered with 0.22 μm filter to remove the large particles, and then immediately dialyzed in deionized water through a dialysis bag for 24 h, during which the deionized water was changed every 3-4 h to fully remove the excess precursors and byproducts. Finally, the red brown CA-PASA CPD powder was obtained after removing the water.

Preparation of CA-EDA CPDs with blue emission. The CA-EDA CPDs was synthesized according to the modified recipe of our previous work.[3] 1.0507 g of citric acid (CA) and 335 μL of ethylenediamine (EDA) was dissolved in DI-water (10 mL). Then, the solution was transferred to a poly(tetrafluoroethylene) (Teflon)-lined autoclave and heated at 200 ºC for 8 h. After the reaction, the reactors were cooled to room temperature naturally. The brown-black and transparent product was subjected to dialysis in order to obtained the CA-EDA CPD powders.

Preparation of NA-OPDA CPDs with red emission. The NA-OPDA CPDs were hydrothermally synthesized according to our previous work.[4] In detail, 0.5 mmol of o-phenylenediamine (OPDA) was dissolved in 10 mL of deionized water (DI water), and added 50 µL of (0.725 mmol) HNO_3 (NA). Then the solution was transferred to a poly (tetrafluoroethylene) Teflon-lined autoclave (25 mL) and heated at 200°C for 10 h. Subsequently, the reactor was cooled to room temperature. The dark-blue solution was obtained through 0.22 µm polyethersulfone membrane to remove large particles and dialyzed in a 500-1000 Da dialysis bag against DI water. Then NA-OPDA CPDs solution was lyophilized for further use.

Synthesis of Ni_3C.The Ni_3C was synthesized according to previous work.[5] 2 mmol of nickel acetate was added into 14 mL of oleylamine under N_2 atmosphere. The above solution was heated to 300°C for 4 h and then cooled to 25°C. The obtained precipitates were centrifuged and subsequently rinsed with ethanol, hexane, and acetone. Finally, the product was dried in 60°C vacuum for 2 h.

Preparation of TiO_2-Pt. TiO_2-Pt was prepared through a photo-reduction deposition method based on previous work.[6] In detail, 250 mg of TiO_2 nanocrystals were dispersed in 60 mL of deionized water. 2 mg of $H_2PtCl_6\cdot 6H_2O$ and 15 mL of CH_3OH were added, and the mixture was then irradiated by a 300 W Xe lamp for 4 h under stirring. After reaction, the product was centrifuged and washed by deionized water and anhydrous ethanol, and dried at 60 ^oC for 24 h in a vacuum oven.

Photocatalytic reactions. Photocatalytic reactions were performed in 25 mL of $MAPbI_3$-saturated solution in a quartz reactor with an exposed irradiation area of 19.63 cm^2. 100 mg of $MAPbI_3$ powders with different amount of CA-PASA CPDs were into the solution. A 300 W Xe lamp (CEL-HXF300) with light intensity of 300 mW $cm^{-2}$was used as the light source with irradiation spectrum controlled by a 420 nm cutoff filter (the photons with wavelength large than 420 nm were allowed to pass). Fan cooling was used on the reactor to keep the temperature of the reactor at 15 ^oC. Before the measurement of H_2 evolution, the mixed suspensions were under ultrasonic condition for 15 min and stirred for 2 h under light irradiation condition until the $MAPbI_3$/CA-PASA CPD hybrid systems reach the dynamic balance. The amount of evolved H_2 was determined by gas chromatograph (CEAULIOHT; GC-7920, Ar as carrier gas). For the photocatalytic performance tests of $MAPbI_3$/CA-EDA CPD or NA-OPDA CPD hybrid, the whole process remained unchanged except for the CPDs.

For SEM, HR-TEM, FTIR and XPS characterizations, the $MAPbI_3$/CA-PASA CPD hybrid was finally obtained via centrifuging, rinsing, and drying.

For Pt-hybrid systems, Pt co-catalyst were hybridized through a photo-reduction process similar to previous work.[6] 2 mg of $H_2PtCl_6·6H_2O$ was added into the $MAPbI_3$/CA-PASA CPD hybrid systems, then the mixed suspensions were dispersed under ultrasonic condition for 15 min and photo-reduced for 3 h under light irradiation condition to obtain the Pt /$MAPbI_3$/CPDs hybrid catalytic systems.

General acceptance of CA-PASA CPDs for HI splitting with different electron-transfer materials. To prove the general acceptance of CA-PASA CPDs for HI splitting with different electron-transfer materials, all the efficient electron-manipulated $MAPbI_3$ photocatalytic systems ($MAPbI_3$/TiO_2-Pt,[6] $MAPbI_3$/graphene,[7] $MAPbI_3$/BP [8] and $MAPbI_3$/Ni_3C [5]) were tested here. The experimental processes were conducted and the optimal content of electron-transfer co-catalysts were added according to the reports. Specifically, 100 mg of $MAPbI_3$ and 50 mg of TiO_2-Pt (or 5 mg of graphene, or 1.2 mg of BP, or 15 mg of Ni_3C) were added to the $MAPbI_3$-saturated HI solution, respectively. For the $MAPbI_3$/TiO_2-Pt and $MAPbI_3$/Ni_3C, the mixtures were heated at 70 °C for 20 min under Ar gas for a preheating treatment that allows the complete dissolution of $MAPbI_3$ precipitates, followed by reprecipitation upon cooling. For the graphene/$MAPbI_3$, the mixtures were photo-reduced under light irradiation for 3 h under vacuum conditions. Then the mixtures were transferred into photocatalytic reactors for the measurement of H_2 evolution. To test the effects of CA-PASA CPDs on these electron-manipulated $MAPbI_3$ photocatalytic systems, 1 mg of CA-PASA CPDs were directly added into these photocatalytic systems without changing other processes.

Calculation of efficiency.

The photocatalytic HI splitting of the CA-PASA CPDs/$MAPbI_3$/Pt hybrid system was carried out under irradiation with the Xe lamp (CEL-HXF300), and light intensity was set to 100 mW cm^{-2} with the aid of a calibrated Si reference solar cell. Irradiation area was set to 0.25 cm^2 by mask. The solar HI splitting efficiency, so-called solar-to-hydrogen (STH) conversion efficiency, is the ratio of solar light converted to break the chemical bonding of HI. Our calculation for HI splitting efficiency is based on the amount of evolved hydrogen.

The H^+ reduction potential to H_2 Was 0 V versus reversible hydrogen electrode (vs RHE), and the I^- oxidation potential to I_3^- was 0.53 V vs RHE. The content of HI was 6.06 M. The I_3^-concentration was estimated as 1.13×10^{-3} M by analyzing the ultraviolet–visible (UV–vis) absorption spectrum of HI aqueous solution (**Fig. S12**) and using the related equation:[1]

$y = 0.0293x + 0.00299$

where x is the concentration of I_3^- and y is the value of the absorbance at 353 nm. The redox potential can be calculated using the Nernst equation. The visible-light-driven HI-splitting efficiency was estimated as follows:

$E\ (2H + 2e^- \rightarrow H_2) = 0 - 0.059/2 \times \lg\ (1/6.06^2) = 0.046$ (vs NHE)

$E\ (3I^- \rightarrow I_3^- + 2e^-) = 0.53 + 0.059/2 \times \lg\ (1.13 \times 10^{-3}/6.06^3) = 0.374$ (vs NHE)

Based on this, the total potential for HI splitting was calculated as 0.374 V−0.046 V = 0.328 V. By using this potential, the HI splitting efficiency was determined by the following equation:

STH efficiency = [Evolved H_2 (mol) × 6.02×10^{23} × 2 × 0.328 (eV) × 1.6×10^{-19}] / [P sol. (W cm^{-2}) × Area (cm^2) × time (s)] × 100%

The apparent quantum efficiency (AQE) experiment of the CA-PASA CPDs/$MAPbI_3$/Pt hybrid system was carried out by a similar procedure of photocatalytic measurement except that a band-passfilter (420 ±10 nm) was used rather than a UV cut-off filter. The AQE was calculated as follows.

AQE (%) = 100 × (number of evolved H_2 molecules × 2) / (number of incident photons)

Ultrafast transient absorption (TA) spectroscopy measurement. The $MAPbI_3$ and hybrid $MAPbI_3$/CA-PASA CPDs films were prepared for TA measurement according to previous work.[9] 200 mg of $MAPbI_3$ photocatalyst powers were dissolved in mixed solvents of DMF and DMSO (4:1 v/v) to form perovskite precursor solution. The $MAPbI_3$ film was deposited on a 2 cm*2 cm quartz substrate through a spin-coating process. The precursor solution was spin-coated onto the quartz in a two-step programme at 600 and 2000 r.p.m. for 2 and 40 s, respectively. During the second step, 200 µl of toluene was dropped on the spinning substrate 20 s prior to the end of the programme. This was followed by annealing the films at 100 °C for 10 min. The $MAPbI_3$/CA-PASA CPDs hybrid films were prepared with similar procedure, but 2 mg of CA-PASA CPDs are added into the $MAPbI_3$ perovskite precursor solution. In order to eliminate the influence of air on TA measurements, both of the $MAPbI_3$ and $MAPbI_3$/CA-PASA CPDs films were covered with another quartz chip and encapsulated by the sealant. All these processes are performed in the N_2-filled glove box.

The femtosecond transient absorption setup (femto-TA-100 of the Time-tech Spectra company) is based on a regenerative amplified Ti:sapphire laser system from Coherent (800 nm, 35 fs, 0.7 uJ/cm^2 per pulse, and 1 kHz repetition rate), nonlinear frequency mixing techniques and the Helios spectrometer (Ultrafast Systems LLC). Briefly, the 800 nm output pulse from the regenerative amplifier was split in two parts with a 50% beam splitter. The transmitted part was used to pump a TOPAS Optical Parametric Amplifier (OPA) which generates a wavelength-tunable laser pulse from 250 nm to 2.5 µm as pump beam. The reflected 800 nm beam was split again into two parts. One part with less than 10% was attenuated with a neutral density filter and focused into a 2 mm thick sapphire window to generate a white light continuum (WLC) from 420 nm to 800 nm used for probe beam. The probe beam was focused with an Al parabolic reflector onto the sample. After the sample, the probe beam was collimated and then focused into a fiber-coupled spectrometer with CMOS sensors and detected at a frequency of 1 KHz. The intensity of the pump pulse used in the experiment was controlled by a variable neutral-density filter wheel. The delay between the pump and probe pulses was controlled by a motorized delay stage. The pump pulses were chopped by a synchronized chopper at 500 Hz and the absorbance change was calculated with two adjacent probe pulses (pump-blocked and pump-unblocked). All experiments were performed at room temperature.

Transient photovoltage (TPV) for charge lifetime measurement. The unencapsulated $MAPbI_3$ and hybrid $MAPbI_3$/CA-PASA CPDs films on ITO substrate were used to measure the charge lifetime dynamics. The sample chamber consisted of a platinum wire gauze electrode (with the transparency of ca. 50%) as top electrode, a mica spacer with thickness of 10 μm as electron isolator, and a glass substrate covered with indium-tin oxide (ITO) as bottom electrode. The samples were sandwiched between the electron isolator and bottom electrode, and excited with a laser pulse (355 nm with pulse width of 5 ns) generated by a third harmonic Nd:YAG laser (Polaris, New Wave Research, Inc.). The Intensity of pulse was adjusted with a neutral grayfilter and measured by an EM500 single-channel joulemeter (Molectron, Inc.). The TPV data were obtained through a 500-MHz digital phosphor oscilloscope (TDS 5054, Tektronix) with a preamplifier.

The *in situ* TPV for studying the photocatalytic reaction mechanism. The *in situ* TPV measurements were conducted under room temperature. We deposited the as-prepared $MAPbI_3$ photocatalysts (1000 mg of $MAPbI_3$ was dispersed in 5 mL of dry hexane) on indium-tin oxide (ITO, 1 cm × 4 cm) glass substrates to prepare the $MAPbI_3$ working electrodes. The $MAPbI_3$ electrodes were covered with a small amount of CA-PASA CPDs to obtain the CA-PASA CPDs/ $MAPbI_3$ hybrid samples. The CA-PASA CPDs were dissolved in dilute isopropanol and deposited through spray process. And then the electrodes were dried in vacuum oven for 2 h. During the testing process, the working electrodes were kept wet with pure ethyl acetate or 1 % HI/ethyl acetate mixed solution (v/v), respectively. These solutions were saturated with N_2 to protect photocatalysts from the influences of O_2. Isopropanol and ethyl acetate were used due to their amity with $MAPbI_3$. The samples were excited by a laser radiation pulse (λ=355 nm, pulse width 5 ns) from a third-harmonic Nd: YAG laser (Polaris II, New Wave Research, Inc.). The photocurrent is the ratio of the photovoltage to the internal resistance of the test systems.

Characterization. Shimadzu 3600 UV-visible-NIR spectrophotometer was used to measure the UV-visible absorption spectra. The PL spectra were collected by a Shimadzu RF-5301 PC spectrometer. PL lifetime (with TCPSC technology) were collected on FLS 920 (Edinburgh). Fourier transfer infrared (FTIR) measurements was obtained from a Nicolet AVATAR 360 FTIR spectrophotometer. Scanning electron microscope (SEM) images were taken using HITACHI SU800 at 3 KV 10 mA. The morphology of the CA-PASA CPDs and $MAPbI_3$ powders on the super thin carbon film was observed by the transmission electron microscopy (TEM), which was a JEM-2100F microscope operated at 200kV with a CCD camera. The XPS spectroscopy was investigated by ESCA LAB 250. The crystallinity and phase of $MAPbI_3$ powders were studied by XRD using a Empyrean Diffractometer with Cu Kα radiation at 40 KV and 40 mA. Ultraviolet photoelectron spectra (UPS) were collected by the spectrometer (PREVAC sp.z.0.0, R3000).

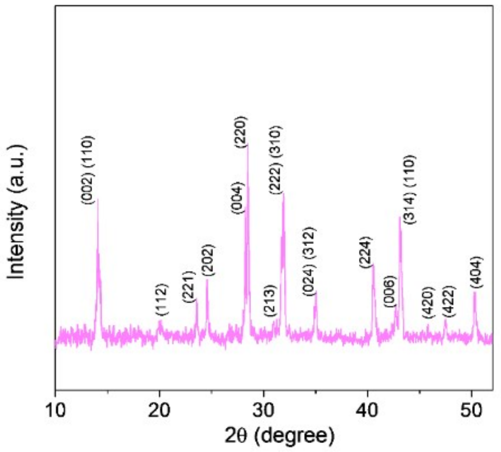

Fig. S1 XRD pattern of as-prepared $MAPbI_3$ powders.

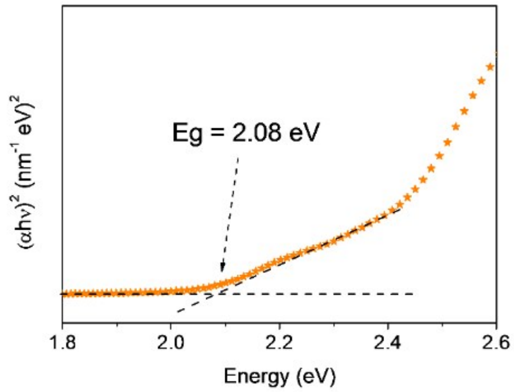

Fig. S2 The plots of $(ah\nu)^2$ vs $h\nu$ calculated from absorption spectrum of CA-PASA CPDs, indicating a E_g of 2.08 eV.

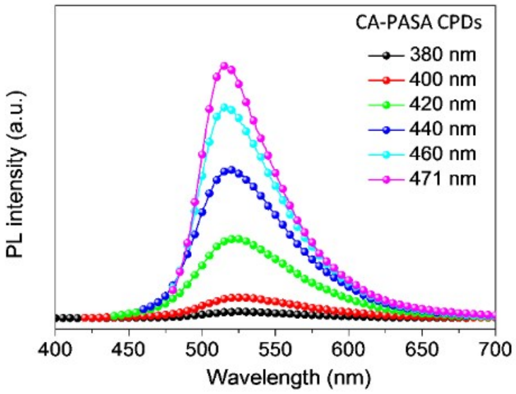

Fig. S3 The PL spectra of CA-PASA CPDs.

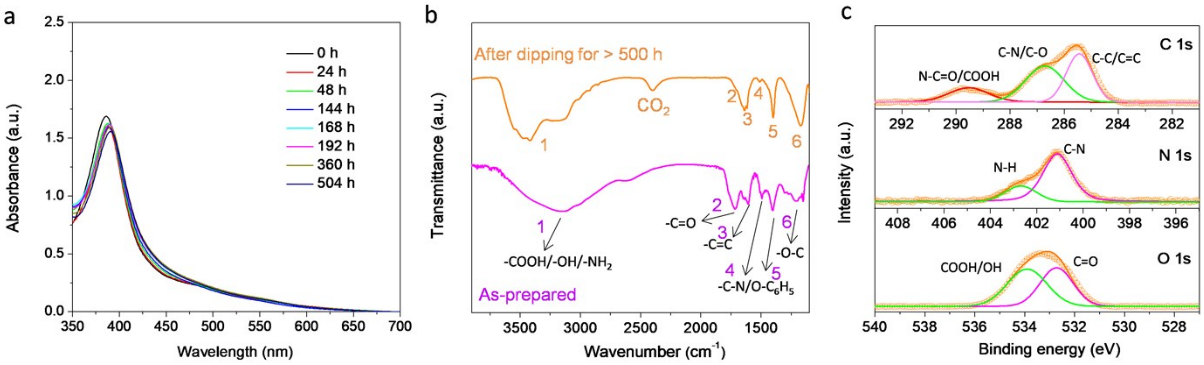

Fig. S4 (a) The absorption spectra of CA-PASA CPDs over time in HI solution. (b) The FTIR of as-prepared CA-PASA CPDs (magenta) and after dipping in HI acid for > 500 h (orange). The chemical groups of CA-PASA CPDs are well-preserved in HI solution for > 500 h. (c) XPS spectra of as-prepared CA-PASA CPDs.

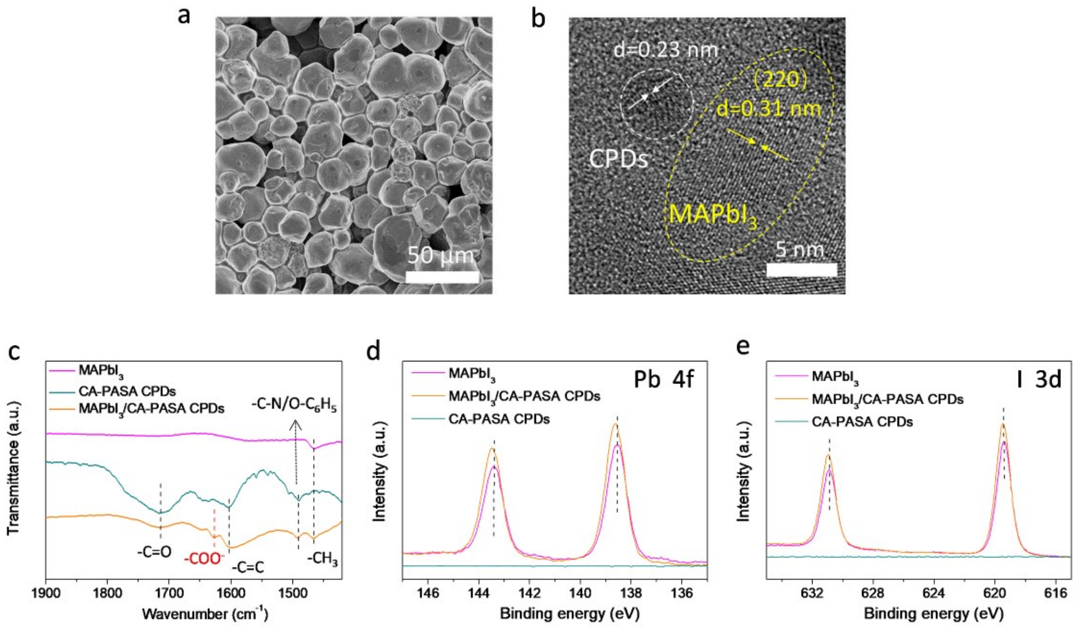

Fig. S5 Studies on the interaction between MAPbI$_3$ and CA-PASA CPDs. (a) SEM and (b) HR-TEM images of MAPbI$_3$/CA-PASA CPD hybrid. (c) FT-IR and (d) - (e) XPS spectra of MAPbI$_3$, CA-PASA CPDs and MAPbI$_3$/CA-PASA CPD hybrid.

As shown in **Fig. S5**b, the crystal fringes of CA-PASA CPDs and MAPbI$_3$ are both observed, indicating the anchor of CPDs on the surface of MAPbI$_3$. Due to the high crystallinity of MAPbI$_3$, their lattice fringes are clearer than that of CPDs. FT-IR and XPS measurements were conducted to study the interaction between MAPbI$_3$ and CA-PASA CPDs. In the FT-IR spectrum of MAPbI$_3$/CA-PASA CPDs (**Fig. S5**c), new peak at 1626 cm^{-1} appears, corresponding to the vibration signal of carboxylate ions (COO$^-$). Besides, the Pb 4f peak of MAPbI$_3$ shifts toward a higher binding energy level for the MAPbI$_3$/CA-PASA CPDs (**Fig. S5**d), while the location of I 3d peak remains unchanged (**Fig. S5**e). The above results suggest coordination bonds of COO-Pb formed between CPD carboxyl moieties and Pb^{2+} ions of MAPbI$_3$; that is, CA-PASA CPDs bind with MAPbI$_3$ mainly by COO−Pb coordination bond.

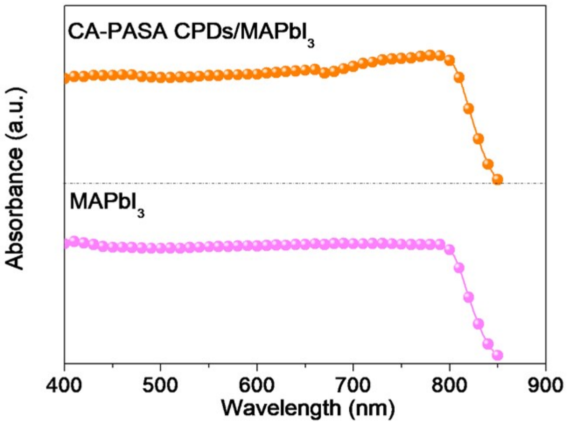

Fig. S6 The comparison of absorption spectra for $MAPbI_3$ and $MAPbI_3$/CA-PASA CPDs hybrid.

Tab. S1 Summary of TRPL triple exponential fitting parameters.[a]

Samples	**τ_1 (ns)**	**f_1 (%)**	**τ_2 (ns)**	**f_2 (%)**	**τ_3 (ns)**	**f_3 (%)**	**χ^2**	**τ_{ave}[b] (ns)**
MAPbI3	0.95	41.2	33.3	39.6	223.7	19.2	0.997	56.5
MAPbI3/CA-PASA CPDs	0.61	73.4	27.5	10.2	193.8	16.4	0.995	35.0

[a] Normalized time-resolved photoluminescence data are fit to the following exponential equation:[10]

$$Intensity = f_1 e^{-t/\tau_1} + f_2 e^{-t/\tau_2} + f_3 e^{-t/\tau_3} + b$$

[b] Average lifetime, τ_{ave}, are calculated by

$$\tau_{ave} = f_1\tau_1 + f_2\tau_2 + f_3\tau_3$$

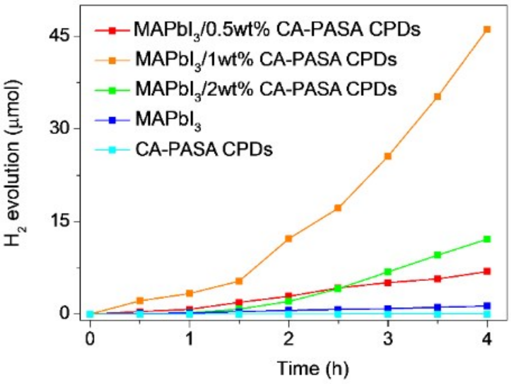

Fig. S7 Photocatalytic performance of $MAPbI_3$, $MAPbI_3$ with different CA-PASA CPD content, and pure CA-PASA CPDs under visible light (λ > 420 nm).

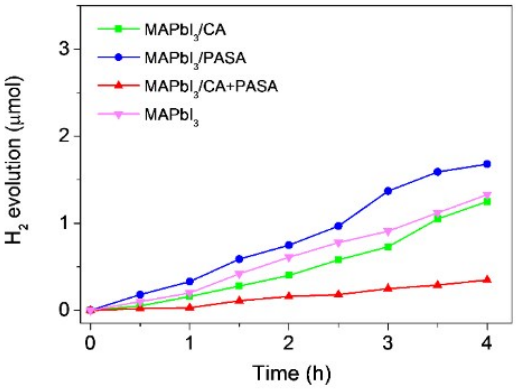

Fig. S8 Photocatalytic performance of $MAPbI_3$ and $MAPbI_3$ with CA-PASA CPD precursors under visible light (λ > 420 nm).

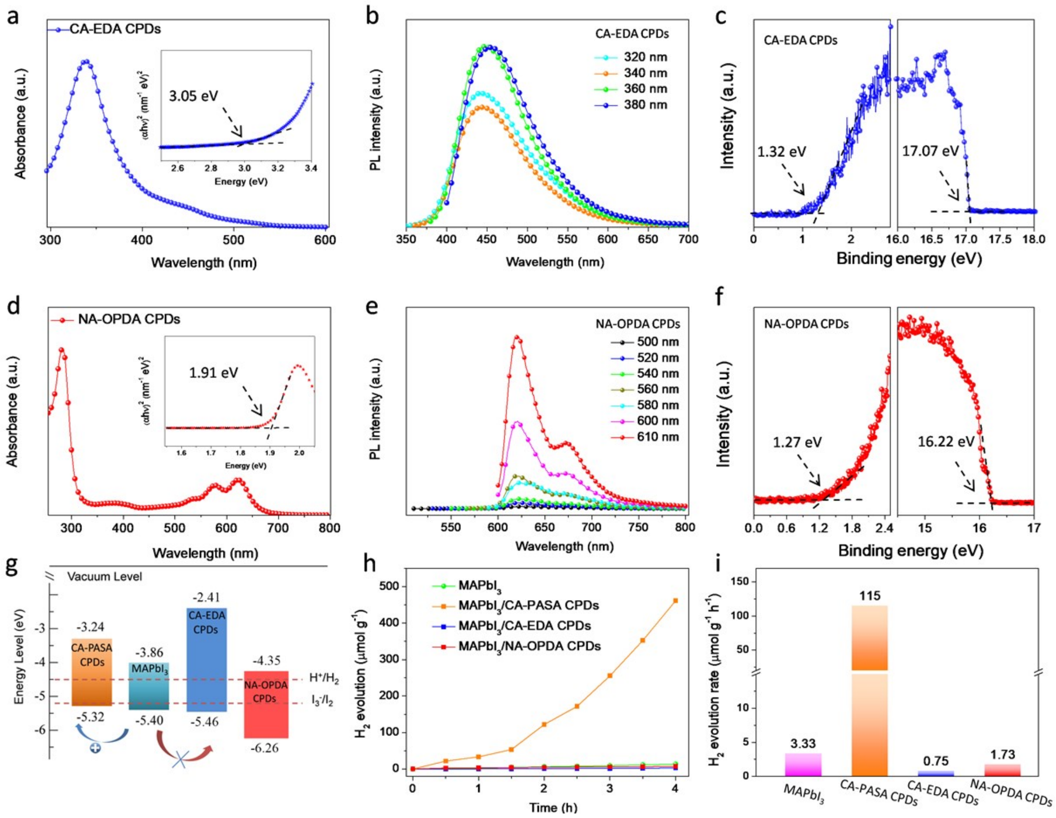

Fig. S9 Characterizations of CA-EDA CPDs and NA-OPDA CPDs. (a)-(c) Characterizations of CA-EDA CPDs with blue emission. (a) Absorption, (b) PL and (c) UPS spectra of CA-EDA CPDs. HOMO = -(21.21-17.07+1.32) eV = -5.46 eV. Insert of (a) is the plots of $(ah\nu)^2$ vs $h\nu$ calculated from absorption spectra of CA-EDA CPDs, indicating a E_g of 3.05 eV. Therefore, the LUMO is -2.41 eV. (d)-(f) Characterizations of NA-OPDA CPDs with red emission. (d) Absorption, (e) PL and (f) UPS spectra of NA-OPDA CPDs. HOMO = -(21.21-16.22+1.27) eV = -6.26 eV. Insert of (d) is the plots of $(ah\nu)^2$ vs $h\nu$ calculated from absorption spectra of NA-OPDA CPDs, indicating a E_g of 1.91 eV. Therefore, the LUMO is -4.35 eV. (g) Schematic energy level diagram of $MAPbI_3$, CA-PASA CPDs, CA-EDA CPDs and NA-OPDA CPDs based on the UPS results. (h) Photocatalytic performance and (i) corresponding H_2 evolution rate of $MAPbI_3$ and $MAPbI_3$ with different CPDs under visible light ($\lambda > 420$ nm).

Based on the energy alignment between $MAPbI_3$ and different CPDs, only the CA-PASA CPDs have matched energy level with $MAPbI_3$ and can extract the holes from $MAPbI_3$, thus leading to long-lifetime electrons in $MAPbI_3$ for enhanced photocatalytic performance.

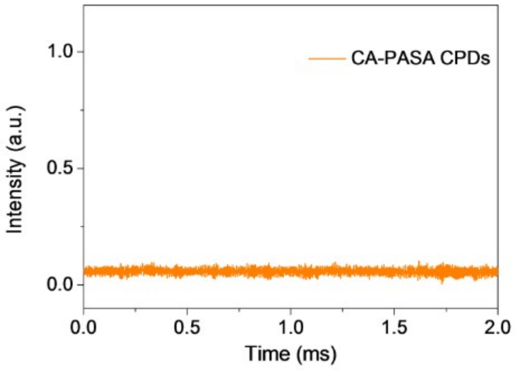

Fig. S10 The in situ TPV of CA-PASA CPDs covered with EtOAc.

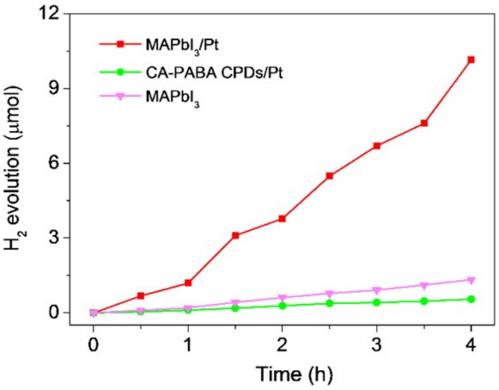

Fig. S11 Photocatalytic performance of MAPbI$_3$, MAPbI$_3$/Pt and CA-PASA CPDs/Pt under visible light (λ > 420 nm).

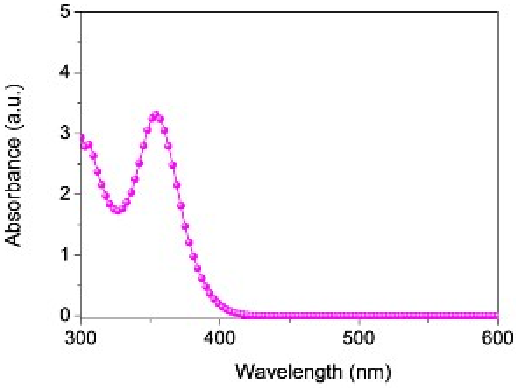

Fig. S12 UV-vis light absorption spectrum of HI aqueous solution which diluted to 1/10 with deionized water.

Tab. S2 A summary of the detail performance parameters of reported metal halide perovskite photocatalysts for H_2 evolution.

Catalysts	**Light source**	**Activity (μmol h^{-1} g^{-1})**	**STH**	**AQE (wavelength)**	**Ref.**
$MAPbI_3$/Pt	100 mWcm^{-2} ($\lambda > 475$nm)	57	0.81%	–	2016 -Nat.Energy[1]
$MAPbI_3/TiO_2$-Pt	200 mWcm^{-2} ($\lambda >420$nm)	1987	0.86%	70% (420 nm)	2018-ACS Energy Lett.[6]
$MAPbI_3$/rGO	300 W $\lambda \geq 420$ nm	894	–	1.4% (450 nm)	2018-Adv. Mater.[7]
$MAPbBr_{3-x}I_x$/Pt	100 mW cm^{-2} ($\lambda \geq 420$ nm)	2605	1.05%	–	2018 -ACS Catal.[11]
Pt-Ta_2O_5/$MAPbBr_3$/ PEDOT:PSS	150 mW cm^{-2} ($\lambda > 420$ nm)	977	–	16.4% (420 nm)	2019-ACS Energy Lett.[9]
$MAPb(I_{1-x}Br_x)_3$	300 mW cm^{-2} ($\lambda \geq 420$ nm)	1471	1.42%	–	2019-Appl. Catal. B[12]
$CsPbBr_{3-x}I_x$/Pt	120 mW cm^{-2} ($\lambda \geq 420$ nm)	1120	–	2.15% (450 nm)	2019-Appl. Catal. B[13]
$Ni_3C/MAPbI_3$	300 W ($\lambda \geq 420$ nm)	2362	0.91%	16.6% (420 nm)	2019-ACS Catal.[5]
$MA_3Bi_2I_9$ /Pt	300 W ($\lambda \geq 400$ nm)	169	0.48%	–	2019-ACS Sustainable Chem. Eng.[14]
$MAPbI_3$/(piezoelectric)	100 mW cm^{-2} ($\lambda \geq 420$ nm)	466	–	–	2019-Adv. Energy Mater.[15]
$MAPbI_3$/BP nanosheets	300 mW cm^{-2} ($\lambda \geq 420$ nm)	3742	0.93%	23.2% (420 nm)	2019-Appl. Catal. B[8]
$PtI_x/[(CH_3)_2NH_2]_3[BiI_6]$	LED 9 mW ($\lambda = 465$ nm)	46.7	–	27.8% (425 nm) 82.8% (465 nm)	2019-Nano Energy[16]
Pt/$MAPbI_3$/CA-PASA CPDs	300 W **($\lambda \geq 420$ nm)**	**11497**	**2.15%**	**53.6 % (420 nm)**	**This work**

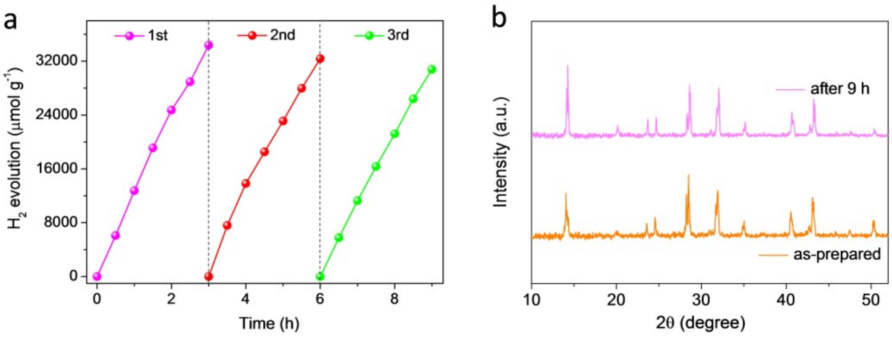

Fig. S13 (a) Three cycles of photocatalytic process were repeated. (b) XRD patterns of the photocatalysts before and after stability test, and tetragonal $MAPbI_3$ phase was maintained after photocatalytic HI splitting reaction.

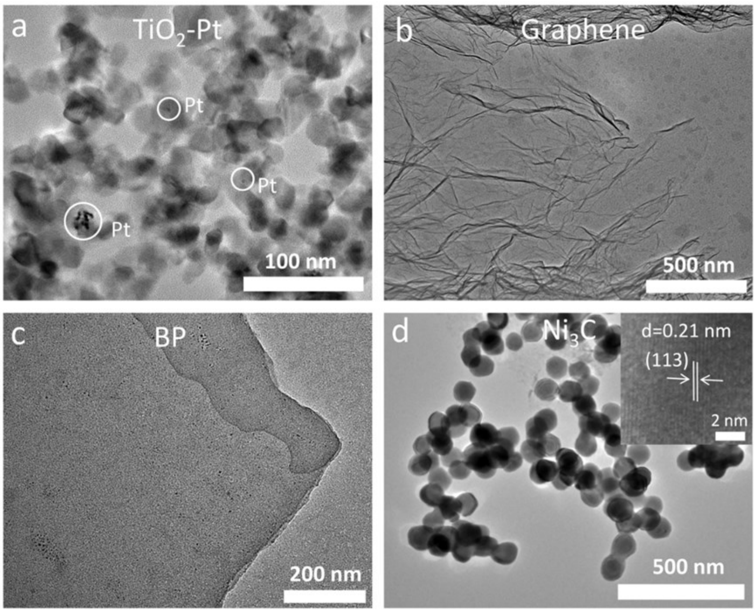

Fig. S14 Morphology characterizations of different electron-transfer materials. TEM images of (a) TiO_2-Pt, (b) graphene, (c) black phosphorus nanosheets and (d) Ni_3C. Insert of (d) is the HR-TEM image of Ni_3C.

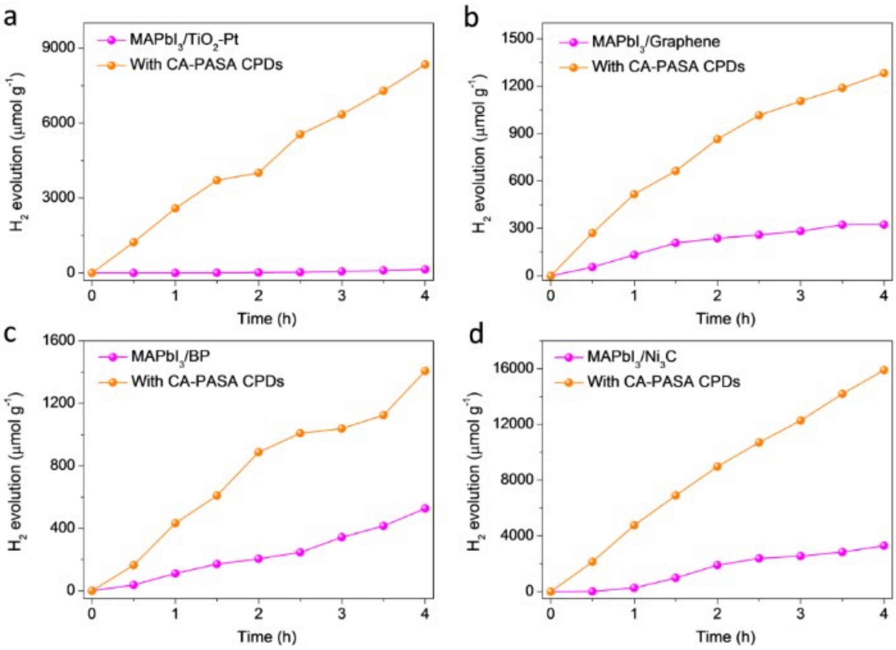

Fig. S15 Photocatalytic performance of (a) $MAPbI_3/TiO_2$-Pt and CA-PASA CPDs/$MAPbI_3/TiO_2$-Pt, (b) $MAPbI_3$/graphene and CA-PASA CPDs/$MAPbI_3$/ Graphene, (c) $MAPbI_3$/BP and CA-PASA CPDs/$MAPbI_3$/BP, (d) $MAPbI_3/Ni_3C$ and CA-PASA CPDs/$MAPbI_3/Ni_3C$.

Reference

1. S. Park, W. J. Chang, C. W. Lee, S. Park, H.-Y. Ahn and K. T. Nam, *Nature Energy*, 2016, **2**.
2. T. Feng, Q. Zeng, S. Lu, X. Yan, J. Liu, S. Tao, M. Yang and B. Yang, *ACS Photonics*, 2017, **5**, 502-510.
3. S. Zhu, Q. Meng, L. Wang, J. Zhang, Y. Song, H. Jin, K. Zhang, H. Sun, H. Wang and B. Yang, *Angew. Chem.*, 2013, **52**, 3953-3957.
4. J. Liu, D. Li, K. Zhang, M. Yang, H. Sun and B. Yang, *Small*, 2018, **14**, 1703919.
5. Z. Zhao, J. Wu, Y.-Z. Zheng, N. Li, X. Li and X. Tao, *ACS Catal.*, 2019, **9**, 8144-8152.
6. X. Wang, H. Wang, H. Zhang, W. Yu, X. Wang, Y. Zhao, X. Zong and C. Li, *ACS Energy Lett.*, 2018, **3**, 1159-1164.
7. Y. Wu, P. Wang, X. Zhu, Q. Zhang, Z. Wang, Y. Liu, G. Zou, Y. Dai, M. H. Whangbo and B. Huang, *Adv. Mater.*, 2018, **30**, 1704342.
8. R. Li, X. Li, J. Wu, X. Lv, Y.-Z. Zheng, Z. Zhao, X. Ding, X. Tao and J.-F. Chen, *Appl. Catal., B*, 2019, **259**, 118075.
9. H. Wang, X. Wang, R. Chen, H. Zhang, X. Wang, J. Wang, J. Zhang, L. Mu, K. Wu, F. Fan, X. Zong and C. Li, *ACS Energy Lett.*, 2018, **4**, 40-47.
10. Q. Zeng, X. Zhang, X. Feng, S. Lu, Z. Chen, X. Yong, S. A. T. Redfern, H. Wei, H. Wang, H. Shen, W. Zhang, W. Zheng, H. Zhang, J. S. Tse and B. Yang, *Adv. Mater.*, 2018, **30**, 1705393.
11. Y. Wu, P. Wang, Z. Guan, J. Liu, Z. Wang, Z. Zheng, S. Jin, Y. Dai, M.-H. Whangbo and B. Huang, *ACS Catal.*, 2018, **8**, 10349-10357.
12. Z. Zhao, J. Wu, Y.-Z. Zheng, N. Li, X. Li, Z. Ye, S. Lu, X. Tao and C. Chen, *Appl. Catal., B*, 2019, **253**, 41-48.
13. Z. Guan, Y. Wu, P. Wang, Q. Zhang, Z. Wang, Z. Zheng, Y. Liu, Y. Dai, M.-H. Whangbo and B. Huang, *Appl. Catal., B*, 2019, **245**, 522-527.
14. Y. Guo, G. Liu, Z. Li, Y. Lou, J. Chen and Y. Zhao, *ACS Sustainable Chem. Eng.*, 2019, **7**, 15080-15085.
15. M. Wang, Y. Zuo, J. Wang, Y. Wang, X. Shen, B. Qiu, L. Cai, F. Zhou, S. P. Lau and Y. Chai, *Adv. Energy Mater.*, 2019, **9**, 1901801.
16. H. Zhao, Y. Li, B. Zhang, T. Xu and C. Wang, *Nano Energy*, 2018, **50**, 665-674.